Article

Exploring the Potential of Water-Soluble Cu(II) Complexes with MPA–CdTe Quantum Dots for Photoinduced Electron Transfer

Niharika Krishna Botcha [1], Rithvik R. Gutha [2], Seyed M. Sadeghi [2] and Anusree Mukherjee [3,*]

1 Department of Chemistry, The University of Alabama in Huntsville, 301 Sparkman Drive, Huntsville, AL 35899, USA; nb0041@uah.edu
2 Department of Physics and Astronomy, The University of Alabama in Huntsville, 301 Sparkman Drive, Huntsville, AL 35899, USA; rithvik.gutha@ii-vi.com (R.R.G.); ss0013@uah.edu (S.M.S.)
3 Department of Chemistry and Geosciences, Jacksonville State University, 700 Pelham Rd N, Jacksonville, AL 36265, USA
* Correspondence: amukherjee@jsu.edu

Abstract: Three water-soluble copper complexes based on the amine/pyridine functionalities were investigated, along with quantum dots, as a catalyst–photosensitizer assembly, respectively, for fundamental understanding of photoinduced electron transfer. Luminescence quenching and lifetime measurements were performed to try and establish the actual process that leads to the quenching, such as electron transfer, energy transfer, or complex formation (static quenching). Cyclic voltammetry and dynamic light scattering experiments were also performed. Irrespective of the similar reduction potentials of the three complexes, very different photoluminescence properties were observed.

Keywords: copper complexes; quantum dots; quenching

1. Introduction

The serious environmental impacts of fossil fuels have made energy-related research the paramount task of our society in the current times [1–3]. Developing alternative and sustainable energies, especially environmentally friendly conversion and storage technologies that address the global energy needs, will be an invaluable mission [2,4,5]. Therefore, many efforts have been made to explore approaches such as artificial photosynthesis system, wherein the overall process consists of light harvesting, charge separation, electron-transfer process, and chemical conversion [2,6]. The most viable method for large-scale growth in carbon-free energy is the light-driven splitting of water into its constituent elements [7,8]. Photocatalytic hydrogen production has been regarded as a promising solution to relieve the crisis triggered by the depletion of fossil fuels [9,10]. To improve the efficiency of hydrogen production, a key subject for overcoming the issues would be the development of an efficient and stable catalytic system with cheap and abundant materials [3,8].

Copper catalysts for proton reduction have recently gained special attention in facilitating solar and electrochemical energy storage via the formation of hydrogen fuel [3,11]. Cu is one of the most widely used metals in human society and, compared with other inexpensive metals (Ni, Co, Mo, etc.), it could be very favorable due to its higher abundance for practical applications [12,13]. Since Cu is earth-abundant and can support well-defined coordination chemistry, in addition to having diverse redox chemistry and rich photochemistry, biomimetic synthetic copper complexes have been investigated for application in hydrogen production [1–3,14–17].

Cu complexes have been explored extensively and used as catalysts for various transformations including CO_2 reduction and water oxidation [3,16]. However, their potential application in catalyzing H_2 production has been less developed [13,18]. Despite this fact, Cu complexes can be utilized for hydrogen evolution reactions, because they display accessible low oxidation states required during the catalytic cycle [19,20]. Cu molecular catalysts

for the development of copper-based molecular systems for H_2 evolution under aqueous conditions have only started to be explored in the past decade [9,21]. Cu complexes can be promising candidates for artificial photosynthesis because of their relatively high reactivity, stability, and relatively low light absorption [2].

Recently, a few mononuclear copper complexes have been reported as homogeneous electrocatalysts for hydrogen production from water [1,13,16,18]. Given the molecular nature of these Cu catalysts, they present an ideal opportunity for the investigation of homogenous photocatalytic hydrogen production with molecular Cu complexes. To date, only a few copper complexes have been reported to be active as molecular catalysts for light-driven or photocatalytic hydrogen evolution reactions (HERs) [3,6,8,11,17,19,21]. In the last decade, the first examples of copper-based molecular catalysts active under photocatalytic HER conditions were reported (Figure 1A,B) [17]. Similarly, in the years after, various copper complexes and varied reaction conditions were employed to successfully produce hydrogen photocatalytically (Figure 1C–K) [3,6,8,11,17–19,21].
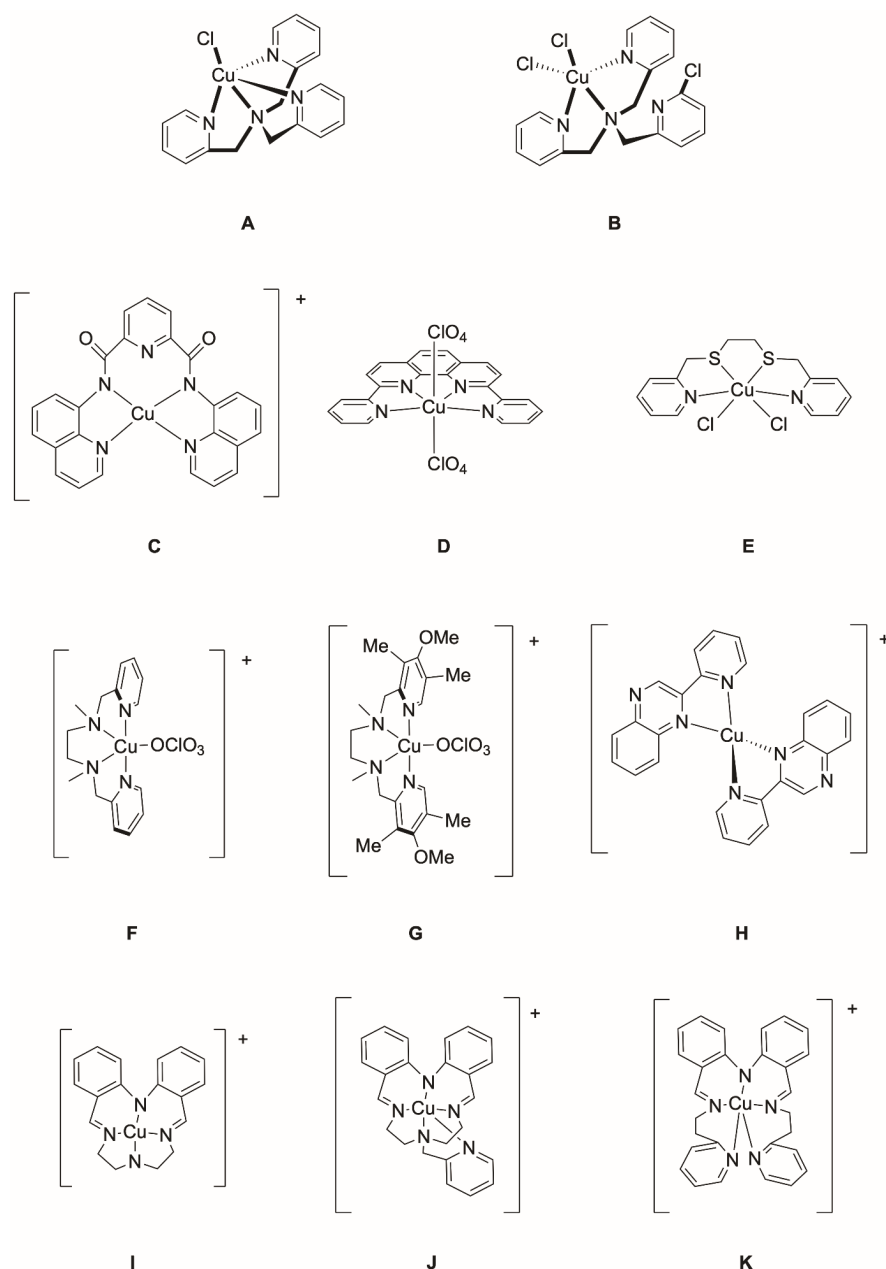

Figure 1. Chemical structures of copper complexes used for photocatalytic H_2 production.

As reported in the previous sections, most of these systems were developed in non-aqueous conditions, except for 1E. In that system, nanomaterials were used as photosensitizers, so quantum dots (QDs), particularly water-soluble QDs, can also be very valuable photosensitizers to explore. QDs have many advantages that are ideal for light-harvesting and electron delivery due to having features such as quantum confinement effect, superior photostability, rich surface-binding properties, a high surface-to-volume ratio, large absorption cross-sections over a broad spectral range, size-dependent absorption properties, long exciton lifetimes, etc. [22,23].

A fundamental step for the photocatalytic system is photoinduced electron transfer (PET). Although there have been reports of Cu photocatalytic systems, the mechanistic investigation of this process is less known. The aim of this report is to investigate a Cu–QD assembly toward the PET pathway. Since all the previously reported Cu HER catalysts are supported by amine/pyridine ligands, we also investigated a similar coordination environment. Therefore, in this paper, we report the investigation of three copper complexes supported by tetradentate ligands with amine and pyridine functionalities (N2/Py2) (Figure 2) toward PET, using QDs. The substituents in the pyridine functionality increase the electron donation ability of **2**, whereas variations in the amine backbone of **3** make the ligand more rigid. With a narrow bandgap of 1.4 eV, CdTe quantum dots stabilized by 3-mercaptopropionic acid (MPA–CdTe QDs) were selected as the photosensitizer owing to their superior properties, as well as their aqueous dispersion and economical advantage [23,24].
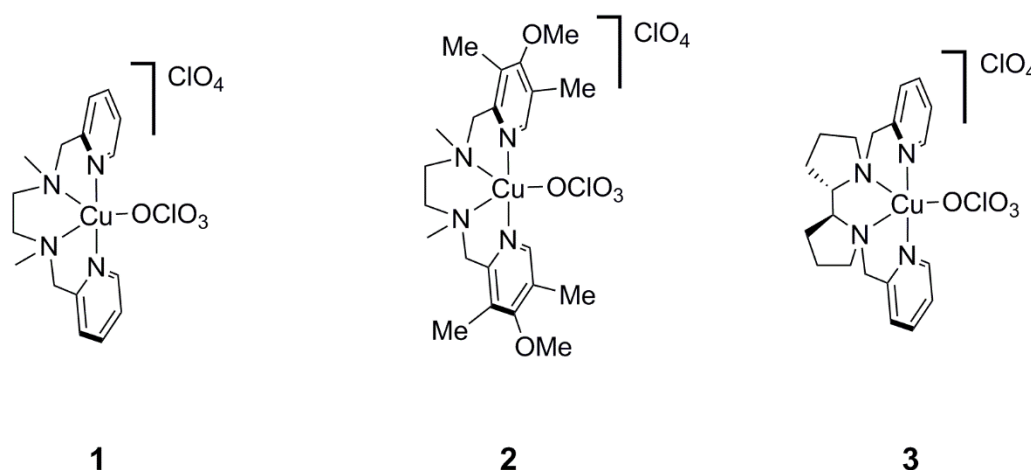

Figure 2. Synthesized copper complexes **1**–**3** with the bispicen (N2/Py2) ligand system.

2. Results and Discussion

Complexes **1**–**3** were synthesized by mixing equimolar amounts of the ligands and copper(II) perchlorate in methanol at room temperature and characterized using analytical methods such as NMR, UV–Vis spectroscopy, ESI–MS, and elemental analyses [25–27].

2.1. Optical Spectroscopy

The electronic absorption spectra for complexes **1**–**3** was recorded in water (Figure 3). Complexes **1**–**3** display broad absorption bands in the visible region at 631 nm, 630 nm, and 593 nm (Table 1), respectively, that were assigned as d–d transitions, as no significant changes were noticed, compared with the MeCN data [26,27]. The minor redshifts observed in water (ca. 5–10 nm) can be attributed to the slight distortion of the geometry of the complexes. The absorption features of all three complexes are characteristic of mononuclear Cu(II) compounds supported by nitrogen-enriched ligands in square pyramidal geometry [26,28,29].
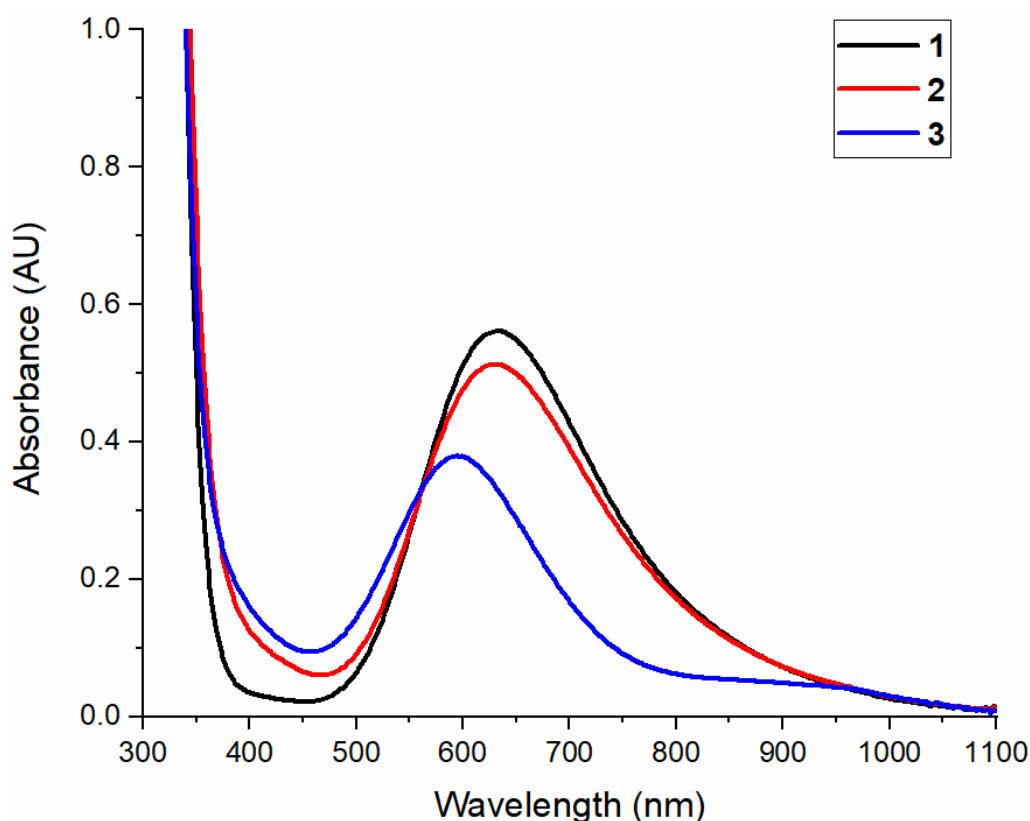
Figure 3. Optical spectra of complexes **1** (black line), **2** (red line), and **3** (blue line) in water using a quartz cuvette with a 1 cm path length. All complexes are dissolved in water to give a 4 mM concentration.

Table 1. Optical and electrochemical parameters for **1–3**.

Complex	Peak Position λ_{max} (nm)	Molar Absorptivity ($M^{-1}cm^{-1}$)	i_{pa}/i_{pc}	$E_{1/2}$ vs. Ag/AgCl (V)	$E_{1/2}$ vs. NHE (V)
1	631	140	0.68	−0.33	−0.042
2	630	128	0.68	−0.40	−0.112
3	593	95	0.67	−0.38	−0.092

2.2. Electrochemical Studies

The redox potentials of **1–3** was measured using cyclic voltammetry (Figures S1–S3). These values give us an insight into the effect of the ligand architecture on the reduction potentials of the complexes. The reduction potential of Cu(II) complexes plays a major role in proton reduction, and these can be tuned using ligand electronics. Systemic variations in the ligand architecture, such as the addition of electron-donating groups and rigidity of the backbone, can affect ligand electronics, which impact the activity and mechanism of proton reduction. All three Cu complexes exhibited fairly reversible cyclic voltammograms with cathodic waves corresponding to the Cu(II)/Cu(I) reduction potential around −0.33 V versus Ag/AgCl for **1**, −0.40 V for **2**, and −0.38 V for **3** (Table 1, Figures S1–S3), respectively, well within the range of other known Cu complexes [6,17,19].

2.3. Luminescence Quenching of QDs by Cu Complexes

The scope of this research is to investigate the roles of these Cu complexes to participate in PET with regard to QDs in water. Understanding the PET phenomenon in a water-soluble photosensitizer system such as the MPA–CdTe QDs will be beneficial for designing an efficient photosensitizer–catalyst assembly. The MPA–CdTe QDs exhibit absorption bands

in the range of 550–650 nm (Figure S4). The photoluminescence of the MPA–CdTe QDs was measured in water at room temperature, following excitation at 514 nm. These QDs are luminescent at room temperature with a maximum emission value of 638 nm (Figure S5). To probe the impact on the luminescent intensity of the MPA–CdTe QDs upon the addition of the copper complexes, solutions of complexes **1**–**3** in water were added to the QDs. The emission intensity of the MPA–CdTe QDs was quenched upon the addition of **1** (Figure 4). The emission quenching could somewhat be correlated to the concentration of the complex with maximum quenching to be observed with the highest concentration. The emission intensity of the MPA–CdTe QDs was also quenched upon the addition of **2** (Figure S6), though no apparent trend could be observed. In both these cases, the amount of quenching was not significant; however, the emission intensity of the MPA–CdTe QDs was drastically quenched upon the addition of **3** (Figure S7). The first two additions of **3** led to a decrease in the intensity of the QDs by about 80–90%. From the third addition of **3** onward, QDs were completely quenched. Stern–Volmer plots (Figures S8–S10) for the luminescence quenching of the MPA–CdTe QDs with **1**–**3** showed that **3** serves as a better quencher when compared with **1**; however, **2** could not be evaluated, as the R^2 value obtained was not in the acceptable range (Table S1).
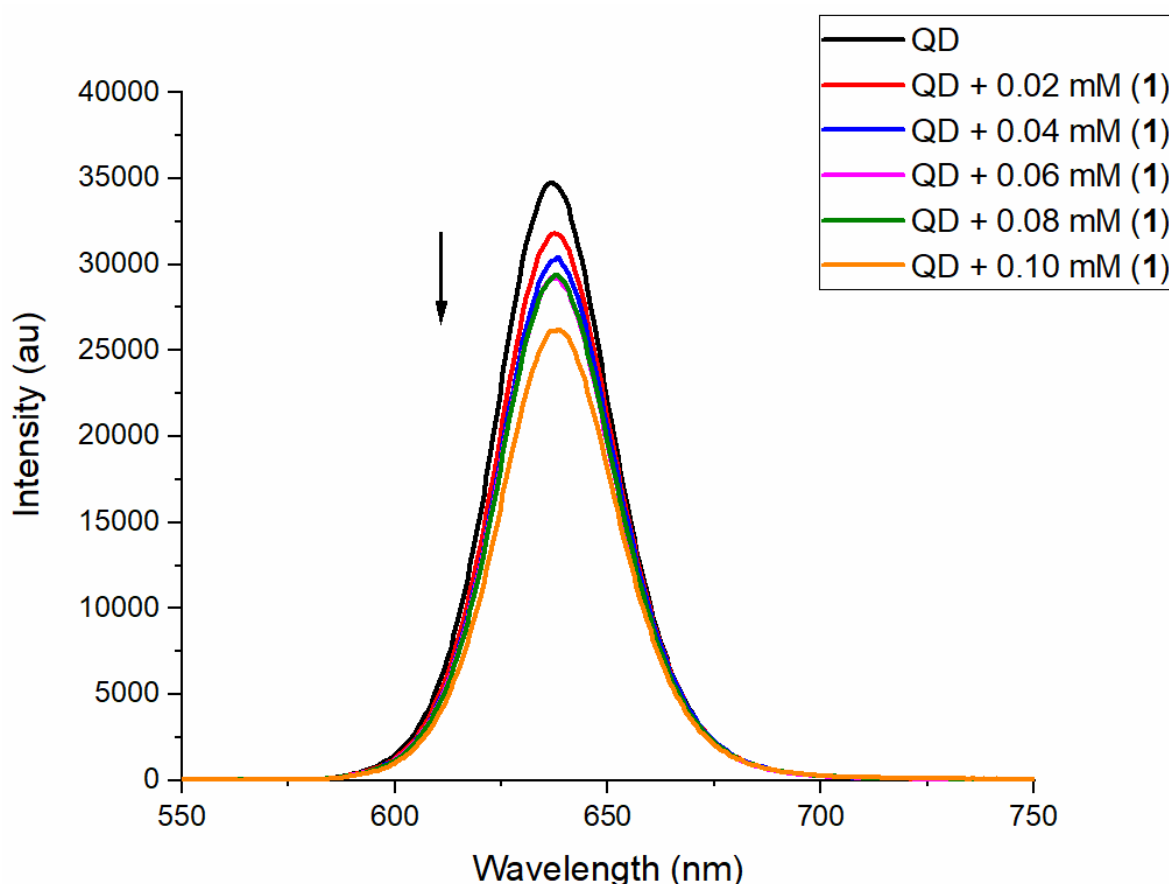

Figure 4. Emission spectra of MPA-CdTe quantum dots (1.4×10^{-6} M, 0.5 mg/mL) with increasing concentration of **1** (0 to 0.10×10^{-3} M) in water (excitation wavelength: 514 nm).

2.4. Lifetime of QDs with Cu Complexes

As a number of processes could lead to quenching, such as energy transfer, electron transfer, or complex formation (static quenching); therefore, the actual process needs to be established. We measured the luminescence lifetime of the MPA–CdTe QDs using a time-correlated single-photon counting (TCSPC) system and monitored the lifetime changes in the presence of Cu complexes. Analysis of the decay revealed that the emission lifetime of the MPA–CdTe QDs did not change with the addition of Cu complexes **1**–**2**

(Figures 5 and S11). As we observed no change in the lifetime, we eliminated the possibility of electron transfer in this case (Table S2) [22,30,31]. Nevertheless, the possibilities of complex formation (static quenching) and energy transfer were still left. The process of energy transfer from the excited MPA–CdTe QDs to the Cu complexes could not be completely eliminated in the case of **1–2**, as the optical spectra (absorption maxima) show overlap with the emission band (maximum) of the MPA–CdTe QDs (Figure S12). However, in the case of **3**, the overlap of the maxima observed is minimal. The lifetime measurements for **3** could not be performed (Figure S13). This was somewhat expected based on the complete emission quenching observed earlier (Figure S7). We believe that the timescale of quenching observed for **3** and the MPA–CdTe QDs is much faster than nanoseconds, which is beyond the capacity of the TCSPC instrument.
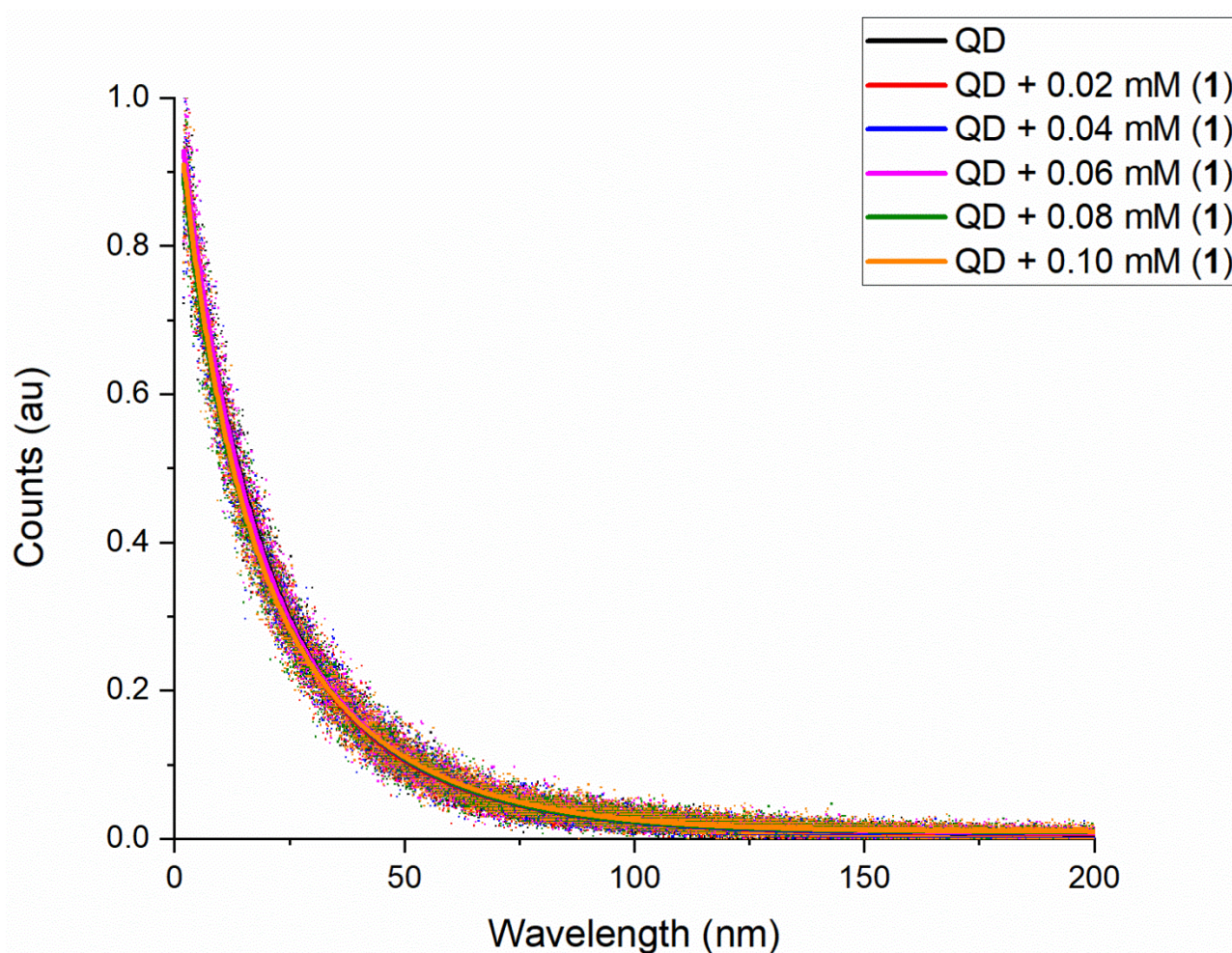

Figure 5. The lifetime of MPA–CdTe quantum dots (1.4×10^{-6} M, 0.5 mg/mL) with increasing concentrations of **1** (0 to 0.10×10^{-3} M) in water (excitation wavelength: 450 nm).

Static quenching is assumed to result from the formation of a quencher (Cu complexes)–fluorophore (quantum dots) complex in the ground state. Shifts of the quantum dots absorption spectrum with added Cu complexes provide evidence of such complex formation [32]. However, that is not the case as observed in the optical spectra measured for MPA–CdTe QDs and complexes **1–3** (Figures S14–S16). Although it was noted, in both the quenching and TCSPC measurements, that the addition of **1–3** leads to a color change in the MPA–CdTe QDs from orange to green even before irradiation by the laser light, no optical change was noted in the spectrum. Another type of static quenching is often observed at high quencher (Cu complexes) concentrations due to the existence of increasing numbers of quencher–fluorophore pairs in which the quencher (Cu complexes) is close enough to

the fluorophore (quantum dots) to instantaneously quench their excited state [33]. Analysis of this type of quenching is less straightforward. However, it can be distinguished from quenching due to true ground-state complex formation because it does not produce changes in the fluorophore (quantum dots) absorption spectrum [32]. The optical data we collected support this phenomenon (Figures S14–S16).

2.5. Dynamic Light Scattering for QDs and Cu Complexes

In a number of cases, it has been demonstrated that the molecular complexes introduced as a catalyst are actually transformed in situ into metal particles or soluble metal colloids [19,20]. It is still difficult to obtain evidence directly since metal colloids or nanoclusters derived from an aggregation process are soluble species and cannot be easily detected [20]. Dynamic light scattering (DLS) is a technique that can be used to identify the presence (or to establish the absence) of nanoparticles or aggregation in solution [2,9,20]. Therefore, DLS measurements can help determine if such aggregations occur with the reactions between the MPA–CdTe QDs and complexes **1**–**3**. When we performed similar experiments with the QDs and Cu complexes (QD + 0.10 mM (**1**–**3**)), nanoparticle sizes could not be measured, as the DLS instrument was not sensitive enough to perform the measurements. QDs are usually in the size range of less than 10 nm, and although the instrument has a 0.1–1000 nm detection range, no measurements could be performed for less than 100 nm, despite optimizing the various conditions.

As a result, we increased the concentration of the Cu complexes in each of the reactions. The concentration of the solutions was doubled to contain 0.20 mM of complexes **1**–**3**. This yielded a measurement of average sizes of 164 ± 50 nm for **1**. This implies that aggregation occurs in the solution and is measurable. To investigate whether aggregation changes with an increase in the concentration of **1**, the solution concentration was increased to contain 0.30 mM and 0.40 mM of **1**. These gave measurements of average sizes of 822 ± 439 nm and 3112 ± 548 nm, respectively (Table 2). Thus, as can be seen, the aggregation increases as the concentration of **1** is increased. The optical spectra of the corresponding measurements also reflect this result (Figure 6). This could also explain the small intensity shifts observed in the optical spectra for **1** earlier (Figure S14).

Table 2. Hydrodynamic sizes for QDs and complexes **1**–**3** from DLS measurements.

Complex	QD + 0.10 mM (Complex) nm	QD + 0.20 mM (Complex) nm	QD + 0.30 mM (Complex) nm	QD + 0.40 mM (Complex) nm
1	N/R	164 (50)	822 (439)	3112 (548)
2	N/R	N/R	473 (72)	460 (84)
3	N/R	N/R	379 (164)	492 (157)

N/R: No measurement could be recorded.

The exact same experiments were performed for QDs with complexes **2**–**3** (Table 2 and S5). However, the trends may not be clear with **2** and **3**. The values of DLS measurements for all Cu complexes indicate that the hydrodynamic sizes vary for each of the complexes. This may be due to different aggregations/agglomerations between QDs and complexes **1**–**3**, resulting in varied sizes. As of now, it can only be said that there is possible aggregation/agglomeration even with the original scale of measurements, though the DLS instrument is not sensitive enough to detect it. However, this observation suggests that most likely the quenching phenomenon reported in this paper is due to static quenching or energy transfer.
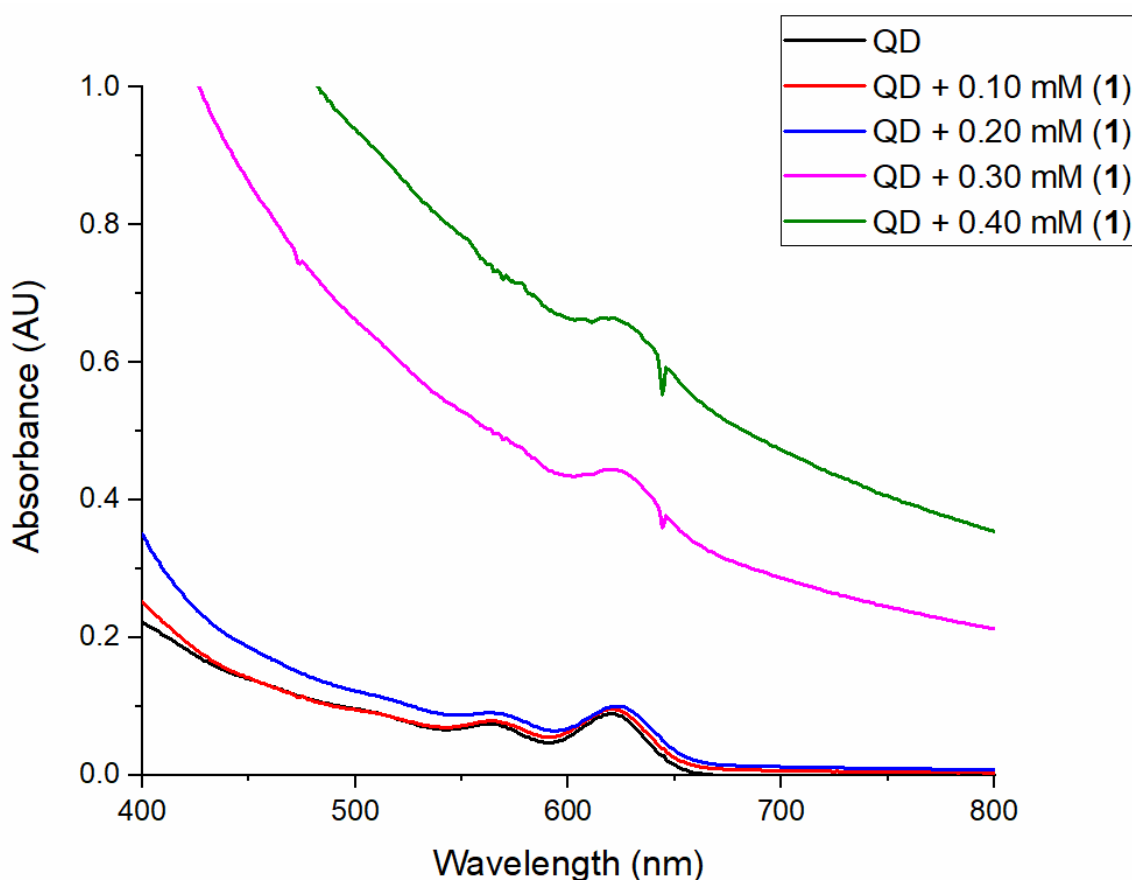
Figure 6. Optical spectra of the MPA–CdTe QDs with increasing concentration of **1**.

3. Materials and Methods

UV–Vis spectroscopy experiments were performed on an Agilent Cary 8454 UV–Vis spectrometer (Agilent, Santa Clara, CA, USA) in a quartz cuvette with a path length of 5 mm. The hydrodynamic diameter of QDs with the complexes was evaluated by dynamic light scattering (DLS), Malvern Zetasizer Nano ZS, Malvern Panalytical Inc. The measurements conditions were as follows: temperature, 25 °C; wavelength of the laser, 633 nm; scattering angle, 173°. The cyclic voltammetry experiments were performed under a nitrogen atmosphere, with Ag/AgCl as the reference electrode and 0.1 M KCl as the supporting electrolyte. In order to measure the potential of the MPA–CdTe, QDs samples were scanned from −1.5 V to +1.5 V in water with a scan rate varying from 100 mV/s to 500 mV/s. Similarly, the complexes were measured in water using a potential window of −1 V to +1 V, with a scan rate varying from 100 mV/s to 500 mV/s. Graphical representation and data analysis were performed using the Origin program (OriginLab Corporation, Northampton, MA, USA).

Water-soluble cadmium telluride quantum dots stabilized by 3-mercaptopropionic acid (MPA-CdTe QDs) were purchased from NNCrystal US Corp (NNCrystal US Corporation, Fayetteville, AR, USA). The emission spectra were recorded using a TE-cooled QEPRO spectrometer from Ocean Optics (Ocean Insight, Orlando, FL, USA). The measurements were performed at room temperature. A continuous-wave laser diode with a 514 nm wavelength was used as an excitation source. The entrance slit was 200 μm, and the slit size was 25 μm. A combination of dichroic mirrors and filters were used to separate the emission of the quantum dots from the laser beam before sending it to the spectrometer. To measure the lifetime of the quantum dots we used a time-correlated single-photon counting (TCSPC) system (Picoquant Time harp 260) combined with a 30 ps pulsed laser with a 450 nm wavelength. All the above emission and lifetime measurements were performed with special optical glass cells with a path length of 10 mm.

3.1. Complex Synthesis

Complexes **1–3** were synthesized following the procedures published in the literature (Supplementary Materials) [25–27,34].

3.2. Sample Preparation and Measurements

The UV–Vis absorption, emission, and lifetime analyses were performed under anaerobic conditions at room temperature as follows: A 1 mL solution of the MPA–CdTe QDs of concentration 1.4×10^{-6} M (0.5 mg/mL) in water was prepared. Then, 4 mM stock solutions of complexes **1–3** in water were also prepared. The MPA–CdTe QD solutions were purged with nitrogen gas for 30 s in a micro cuvette (10 mm pathlength), whereas complexes **1–3** stock solutions were purged with nitrogen gas for 90 s. To the MPA–CdTe QD solution in the cuvette, an aliquot of 10 µL of the 4 mM stock solution of complexes **1–3** was added with the help of a gas-tight syringe.

4. Conclusions

Photoluminescence properties of MPA–CdTe QDs in the presence of copper complexes were investigated in detail, in order to gain a fundamental understanding of their prospects for potential photocatalytic systems. Unfortunately, complexes **1–2** investigated in this publication did not show promising results, as they were unable to reduce the lifetime of QDs. Data suggest that the slight quenching observed for **1–2** arises because of static quenching or energy transfer. Surprisingly, changing the ligand architecture by having a rigid backbone (**3** compared to **1–2**) did lead to a significant change in the decay lifetime of the QDs. However, because of limitations, the exact data could not be ascertained. Based on our observations, measurements for **3** will need to be performed using more sensitive instruments or techniques such as ultrafast spectroscopy and transmission electron microscopy. Based on our findings, we can conclude that the MPA–CdTe QDs are not a suitable photosensitizer to study PET for these Cu complexes. This is somewhat surprising, as the bandgap of these QDs matches well with the potentials of Cu complexes (Figures S17 and S18) [25,34]. These results suggest that designing a Cu–QD system for artificial photosynthesis is much more complicated. As shown in the energy scheme (Figure S18), having the reduction potentials of Cu complexes match with the bandgap of the QDs does not always lead to PET.

Supplementary Materials: The following supporting information can be downloaded at: https://www.mdpi.com/article/10.3390/catal12040422/s1, Figure S1: Cyclic Voltammogram of **1** in water under N_2 with Ag/AgCl as the reference electrode and 0.1 M KCl as the supporting electrolyte; Figure S2: Cyclic Voltammogram of **2** in water under N_2 with Ag/AgCl as the reference electrode and 0.1 M KCl as the supporting electrolyte; Figure S3: Cyclic Voltammogram of **3** in water under N_2 with Ag/AgCl as the reference electrode and 0.1 M KCl as the supporting electrolyte; Figure S4: UV-Vis absorption spectra of MPA-CdTe QDs (2.8×10^{-6} M, 1 mg/mL); Figure S5: Emission spectra of MPA-CdTe QDs (1.4×10^{-6} M, 0.5 mg/mL); Figure S6: Emission spectra of MPA-CdTe quantum dots (1.4×10^{-6} M, 0.5 mg/mL) with increasing concentration of **2** (0 to 0.10×10^{-3} M) in water (excitation wavelength: 514 nm); Figure S7: Emission spectra of MPA-CdTe quantum dots (1.4×10^{-6} M, 0.5 mg/mL) with increasing concentration of **3** (0 to 0.10×10^{-3} M) in water (excitation wavelength: 514 nm); Figure S8: Stern-Volmer plot for the luminescence quenching of MPA-CdTe QDs with **1**; Figure S9: Stern-Volmer plot for the luminescence quenching of MPA-CdTe QDs with **2**; Figure S10: Stern-Volmer plot for the luminescence quenching of MPA-CdTe QDs with **3**; Figure S11: The lifetime of MPA-CdTe quantum dots (1.4×10^{-6} M, 0.5 mg/mL) with increasing concentrations of **2** (0 to 0.10×10^{-3} M) in water (excitation wavelength: 450 nm); Figure S12: Overlay of the absorption maxima of the complexes **1-3** (scale on right) and the emission maximum of the MPA-CdTe QDs (scale on left); Figure S13: The lifetime of MPA-CdTe quantum dots (1.4×10^{-6} M, 0.5 mg/mL) with increasing concentrations of **3** (0 to 0.10×10^{-3} M) in water (excitation wavelength: 450 nm); Figure S14: UV-Vis absorption spectra of MPA-CdTe quantum dots (1.4×10^{-6} M, 0.5 mg/mL) with increasing concentration of **1** (0 to 0.10×10^{-3} M) in water; Figure S15: UV-Vis absorption spectra of MPA-CdTe quantum dots (1.4×10^{-6} M, 0.5 mg/mL) with increasing

concentration of **2** (0 to 0.10×10^{-3} M) in water; Figure S16: UV-Vis absorption spectra of MPA-CdTe quantum dots (1.4×10^{-6} M, 0.5 mg/mL) with increasing concentration of **3** (0 to 0.10×10^{-3} M) in water; Figure S17: Cyclic Voltammogram of MPA-CdTe QDs in water under N2 with Ag/AgCl as the reference electrode and 0.1 M KCl as the supporting electrolyte; Figure S18: Bandgap (vs. NHE) of the MPA-CdTe quantum dots and the reduction potentials (vs. NHE) of the complexes **1**–**3**; Table S1: The Stern–Volmer quenching constant Ksv for the complexes **1** and **3**; Table S2: Mean lifetimes of the quantum dots in the presence of complexes **1**–**2**; Table S3: Biexponential fit parameters and mean lifetimes for **1**; Table S4: Biexponential fit parameters and mean lifetimes for **2**; Table S5: Hydrodynamic sizes for QDs and complexes **1**–**3** from DLS measurements [35].

Author Contributions: Conceptualization, A.M. and N.K.B.; methodology, A.M. and N.K.B.; validation, A.M., S.M.S., N.K.B., and R.R.G.; formal analysis, A.M., S.M.S., N.K.B., and R.R.G.; investigation, A.M., S.M.S., N.K.B., and R.R.G.; resources, A.M. and S.M.S.; writing—original draft preparation, N.K.B.; writing—review and editing, A.M., S.M.S., N.K.B., and R.R.G.; visualization, A.M. and N.K.B.; supervision, A.M.; project administration, A.M.; funding acquisition, A.M. and S.M.S. All authors have read and agreed to the published version of the manuscript.

Data Availability Statement: The data presented in this study are available on request from the corresponding author.

Conflicts of Interest: The authors declare no conflict of interest.

References

1. Lei, H.; Fang, H.; Han, Y.; Lai, W.; Fu, X.; Cao, R. Reactivity and Mechanism Studies of Hydrogen Evolution Catalyzed by Copper Corroles. *ACS Catal.* **2015**, *5*, 5145–5153. [CrossRef]
2. Liu, S.; Lei, Y.-J.; Xin, Z.-J.; Lu, Y.-B.; Wang, H.-Y. Water Splitting Based on Homogeneous Copper Molecular Catalysts. *J. Photochem. Photobiol. A Chem.* **2018**, *355*, 141–151. [CrossRef]
3. Abudayyeh, A.M.; Schott, O.; Feltham, H.L.C.; Hanan, G.S.; Brooker, S. Copper Catalysts for Photo- and Electro-Catalytic Hydrogen Production. *Inorg. Chem. Front.* **2021**, *8*, 1015–1029. [CrossRef]
4. Cook, T.R.; Dogutan, D.K.; Reece, S.Y.; Surendranath, Y.; Teets, T.S.; Nocera, D.G. Solar Energy Supply and Storage for the Legacy and Nonlegacy Worlds. *Chem. Rev.* **2010**, *110*, 6474–6502. [CrossRef]
5. Chu, S.; Majumdar, A. Opportunities and Challenges for a Sustainable Energy Future. *Nature* **2012**, *488*, 294–303. [CrossRef]
6. Majee, K.; Patel, J.; Das, B.; Padhi, S.K. μ-Pyridine-Bridged Copper Complex with Robust Proton-Reducing Ability. *Dalton Trans.* **2017**, *46*, 14869–14879. [CrossRef]
7. Tong, L.; Duan, L.; Zhou, A.; Thummel, R.P. First-Row Transition Metal Polypyridine Complexes That Catalyze Proton to Hydrogen Reduction. *Coord. Chem. Rev.* **2020**, *402*, 213079. [CrossRef]
8. Xie, Z.-L.; Jiang, W.-X.; Zhan, S.-Z.; Wu, S.-P. Design, Synthesis and Characterization of a Co-Photocatalyst Based on a Copper (II) Complex of S,S′-Bis(2-Pyridylmethyl)-1,2-Thioethane for Hydrogen Production under Visible Light. *Inorg. Chem. Commun.* **2019**, *107*, 107464. [CrossRef]
9. Cao, S.; Wang, C.-J.; Wang, G.-Q.; Chen, Y.; Lv, X.-J.; Fu, W.-F. Visible Light Driven Photo-Reduction of Cu^{2+} to Cu_2O to Cu in Water for Photocatalytic Hydrogen Production. *RSC Adv.* **2020**, *10*, 5930–5937. [CrossRef]
10. Du, P.; Eisenberg, R. Catalysts Made of Earth-Abundant Elements (Co, Ni, Fe) for Water Splitting: Recent Progress and Future Challenges. *Energy Environ. Sci.* **2012**, *5*, 6012. [CrossRef]
11. Drosou, M.; Kamatsos, F.; Ioannidis, G.; Zarkadoulas, A.; Mitsopoulou, C.A.; Papatriantafyllopoulou, C.; Tzeli, D. Reactivity and Mechanism of Photo- and Electrocatalytic Hydrogen Evolution by a Diimine Copper(I) Complex. *Catalysts* **2020**, *10*, 1302. [CrossRef]
12. Fukuzumi, S.; Lee, Y.-M.; Nam, W. Thermal and Photocatalytic Production of Hydrogen with Earth-Abundant Metal Complexes. *Coord. Chem. Rev.* **2018**, *355*, 54–73. [CrossRef]
13. Liu, X.; Cui, S.; Sun, Z.; Du, P. Robust and Highly Active Copper-Based Electrocatalyst for Hydrogen Production at Low Overpotential in Neutral Water. *Chem. Commun.* **2015**, *51*, 12954–12957. [CrossRef] [PubMed]
14. Mirica, L.M.; Ottenwaelder, X.; Stack, T.D.P. Structure and Spectroscopy of Copper−Dioxygen Complexes. *Chem. Rev.* **2004**, *104*, 1013–1046. [CrossRef] [PubMed]
15. Lewis, E.A.; Tolman, W.B. Reactivity of Dioxygen−Copper Systems. *Chem. Rev.* **2004**, *104*, 1047–1076. [CrossRef]

16. Zhang, P.; Wang, M.; Yang, Y.; Yao, T.; Sun, L. A Molecular Copper Catalyst for Electrochemical Water Reduction with a Large Hydrogen-Generation Rate Constant in Aqueous Solution. *Angew. Chem. Int. Ed.* **2014**, *53*, 13803–13807. [CrossRef]

17. Wang, J.; Li, C.; Zhou, Q.; Wang, W.; Hou, Y.; Zhang, B.; Wang, X. Photocatalytic Hydrogen Evolution by Cu(II) Complexes. *Dalton Trans.* **2016**, *45*, 5439–5443. [CrossRef]

18. Xin, Z.-J.; Liu, S.; Li, C.-B.; Lei, Y.-J.; Xue, D.-X.; Gao, X.-W.; Wang, H.-Y. Hydrogen Production in a Neutral Aqueous Solution with a Water-Soluble Copper Complex. *Int. J. Hydrog. Energy* **2017**, *42*, 4202–4207. [CrossRef]

19. Kankanamalage, P.H.A.; Ekanayake, D.M.; Singh, N.; de Morais, A.C.P.; Mazumder, S.; Verani, C.N.; Mukherjee, A.; Lanznaster, M. Effect of Ligand Substituents on Nickel and Copper [N_4] Complexes: Electronic and Redox Behavior, and Reactivity towards Protons. *New J. Chem.* **2019**, *43*, 12795–12803. [CrossRef]

20. Artero, V.; Fontecave, M. Solar Fuels Generation and Molecular Systems: Is It Homogeneous or Heterogeneous Catalysis? *Chem. Soc. Rev.* **2013**, *42*, 2338–2356. [CrossRef]

21. Dalle, K.E.; Warnan, J.; Leung, J.J.; Reuillard, B.; Karmel, I.S.; Reisner, E. Electro- and Solar-Driven Fuel Synthesis with First Row Transition Metal Complexes. *Chem. Rev.* **2019**, *119*, 2752–2875. [CrossRef] [PubMed]

22. Liu, C.; Qiu, F.; Peterson, J.J.; Krauss, T.D. Aqueous Photogeneration of H_2 with CdSe Nanocrystals and Nickel Catalysts: Electron Transfer Dynamics. *J. Phys. Chem. B* **2015**, *119*, 7349–7357. [CrossRef] [PubMed]

23. Li, Z.-J.; Li, X.-B.; Wang, J.-J.; Yu, S.; Li, C.-B.; Tung, C.-H.; Wu, L.-Z. A Robust "Artificial Catalyst" in Situ Formed from CdTe QDs and Inorganic Cobalt Salts for Photocatalytic Hydrogen Evolution. *Energy Environ. Sci.* **2013**, *6*, 465–469. [CrossRef]

24. Wang, F.; Wang, W.-G.; Wang, X.-J.; Wang, H.-Y.; Tung, C.-H.; Wu, L.-Z. A Highly Efficient Photocatalytic System for Hydrogen Production by a Robust Hydrogenase Mimic in an Aqueous Solution. *Angew. Chem. Int. Ed.* **2011**, *50*, 3193–3197. [CrossRef]

25. Botcha, N.K. *Chemical Oxidation and Photoinduced Electron Transfer by Nickel and Copper Complexes: A Dissertation*; The University of Alabama in Huntsville: Huntsville, AL, USA, 2021.

26. Khazanov, T.M.; Botcha, N.K.; Yergeshbayeva, S.; Shatruk, M.; Mukherjee, A. Investigating Reactivity and Electronic Structure of Copper(II)-Polypyridyl Complexes and Hydrogen Peroxide. *Inorg. Chim. Acta* **2021**, *516*, 120168. [CrossRef]

27. Singh, N.; Botcha, N.K.; Jones, T.M.; Ertem, M.Z.; Niklas, J.; Farquhar, E.R.; Poluektov, O.G.; Mukherjee, A. Reactivity of Bio-Inspired Cu(II) (N2/Py2) Complexes with Peroxide at Room Temperature. *J. Inorg. Biochem.* **2019**, *197*, 110674. [CrossRef]

28. Singh, N.; Niklas, J.; Poluektov, O.; Van Heuvelen, K.M.; Mukherjee, A. Mononuclear Nickel (II) and Copper (II) Coordination Complexes Supported by Bispicen Ligand Derivatives: Experimental and Computational Studies. *Inorg. Chim. Acta* **2017**, *455*, 221–230. [CrossRef]

29. Pella, B.J.; Niklas, J.; Poluektov, O.G.; Mukherjee, A. Effects of Denticity and Ligand Rigidity on Reactivity of Copper Complexes with Cumyl Hydroperoxide. *Inorg. Chim. Acta* **2018**, *483*, 71–78. [CrossRef]

30. Gimbert-Suriñach, C.; Albero, J.; Stoll, T.; Fortage, J.; Collomb, M.-N.; Deronzier, A.; Palomares, E.; Llobet, A. Efficient and Limiting Reactions in Aqueous Light-Induced Hydrogen Evolution Systems Using Molecular Catalysts and Quantum Dots. *J. Am. Chem. Soc.* **2014**, *136*, 7655–7661. [CrossRef]

31. Boulesbaa, A.; Issac, A.; Stockwell, D.; Huang, Z.; Huang, J.; Guo, J.; Lian, T. Ultrafast Charge Separation at CdS Quantum Dot/Rhodamine B Molecule Interface. *J. Am. Chem. Soc.* **2007**, *129*, 15132–15133. [CrossRef]

32. Fraiji, L.K.; Hayes, D.M.; Werner, T.C. Static and Dynamic Fluorescence Quenching Experiments for the Physical Chemistry Laboratory. *J. Chem. Educ.* **1992**, *69*, 424. [CrossRef]

33. Lakowicz, J.R. *Principles of Fluorescence Spectroscopy*; Springer: Boston, MA, USA, 1983. [CrossRef]

34. Botcha, N.K.; Gutha, R.R.; Sadeghi, S.M.; Mukherjee, A. Synthesis of Water-Soluble Ni(II) Complexes and Their Role in Photo-Induced Electron Transfer with MPA-CdTe Quantum Dots. *Photosynth. Res.* **2019**, *143*, 143–153. [CrossRef] [PubMed]

35. Yu, W.W.; Qu, L.; Guo, W.; Peng, X. Experimental Determination of the Extinction Coefficient of CdTe, CdSe, and CdS Nanocrystals. *Chem. Mater.* **2003**, *15*, 2854–2860. [CrossRef]